

# CO<sub>2</sub> on Graphene: Benchmarking Computational Approaches to Noncovalent Interactions

Christopher Ehlert,\* Anna Piras, and Ganna Gryn'ova\*

Cite This: *ACS Omega* 2023, 8, 35768–35778

Read Online

ACCESS |



Metrics &amp; More

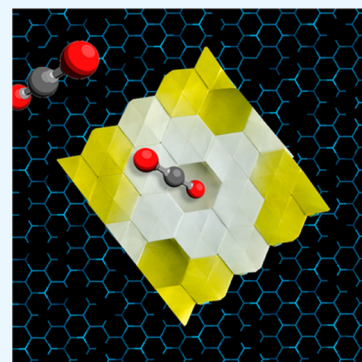


Article Recommendations



Supporting Information

**ABSTRACT:** Designing and optimizing graphene-based gas sensors *in silico* entail constructing appropriate atomistic representations for the physisorption complex of an analyte on an infinite graphene sheet, then selecting accurate yet affordable methods for geometry optimizations and energy computations. In this work, diverse density functionals (DFs), coupled cluster theory, and symmetry-adapted perturbation theory (SAPT) in conjunction with a range of finite and periodic surface models of bare and supported graphene were tested for their ability to reproduce the experimental adsorption energies of CO<sub>2</sub> on graphene in a low-coverage regime. Periodic results are accurately reproduced by the interaction energies extrapolated from finite clusters to infinity. This simple yet powerful scheme effectively removes size dependence from the data obtained using finite models, and the latter can be treated at more sophisticated levels of theory relative to periodic systems. While for small models inexpensive DFs such as PBE-D3 afford surprisingly good agreement with the gold standard of quantum chemistry, CCSD(T), interaction energies closest to experiment are obtained by extrapolating the SAPT results and with nonlocal van der Waals functionals in the periodic setting. Finally, none of the methods and models reproduce the experimentally observed CO<sub>2</sub> tilted adsorption geometry on the Pt(111) support, calling for either even more elaborate theoretical approaches or a revision of the experiment.



## INTRODUCTION

Among practical applications of graphene—a two-dimensional sheet of sp<sup>2</sup>-carbon atoms arranged in a honeycomb lattice<sup>1–3</sup>—detection of small gaseous molecules is arguably most readily geared toward viable real-life implementation.<sup>4–8</sup> Development and optimization of graphene-based gas sensors, which typically operate via (non)covalent interactions of adsorbates with the graphene surface, greatly benefit from theoretical insights into the strengths and nature of these interactions.<sup>9</sup> Examples of the properties studied *in silico* include adsorption geometries, energies, and charge transfer of small molecules (H<sub>2</sub>O, NO, NO<sub>2</sub>, NH<sub>3</sub>, and CO) adsorbed on graphene;<sup>10</sup> selectivity of NH<sub>3</sub> detection with graphene nanoribbons;<sup>11</sup> the role of adsorbate concentration;<sup>12</sup> and surface defects<sup>13</sup> in the adsorption of CO<sub>2</sub> and CO on graphene. In these studies, graphene and its derivatives were modeled as periodic systems; however, an infinite graphene sheet can instead be represented by a finite molecular fragment. For example, in a joint theoretical and experimental study on the adsorption of organic molecules on graphene, averaged *ab initio* molecular dynamics energies obtained with nonlocal van der Waals functionals were in excellent agreement with empirical data.<sup>14</sup>

Choosing an appropriate model of the adsorbate–surface complex in conjunction with an electronic structure theory method, which affords an efficient sampling of adsorption geometries for a given adsorbate concentration regime, is a key to accurately simulate graphene-based gas sensors.<sup>9</sup> Periodic representation of the surface can be advantageously free of

defects and edge effects; yet, on an *ab initio* level it is usually feasible only at the local density or generalized gradient approximations (LDA and GGA, respectively) of density functional theory (DFT), which cannot describe dispersive interactions without empirical corrections or nonlocal functional extensions. While more high-level density functionals, periodic second-order perturbation theory (MP2), random phase approximation (RPA), and the GW approach are available and able to address the aforementioned limitations of LDA and GGA DFT, they generally come at a prohibitively high computational cost.<sup>9</sup> This is particularly the case for adsorption in the low-coverage regime, where large surface slab models are required, in addition to large vacuum gaps along the normal directions of the surfaces. Finite cluster models, on the other hand, can be treated with a broad spectrum of wave-function-based methods, as well as density functionals from the higher rungs of the Jacob's ladder.<sup>15,16</sup> Unfortunately, these models suffer from artificial edge effects and heavy size dependence of the resulting computed properties. Several studies performed a comparison of cluster and periodic models for studying

Received: May 10, 2023

Accepted: September 5, 2023

Published: September 20, 2023



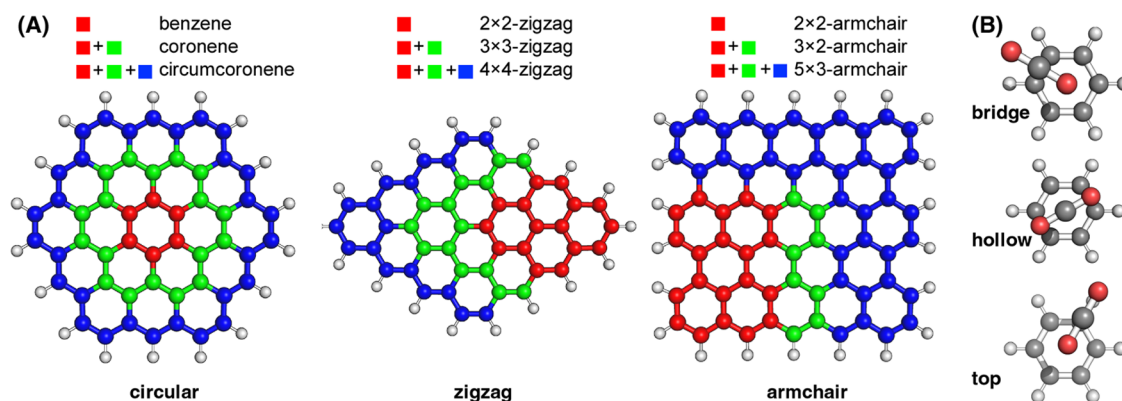


**Figure 1.** (A) Graphene surface models: the smallest model in red, a mid-sized model in red and green, and a large model in red, green, and blue. (B) Principal adsorption sites are shown for a parallel orientation of CO<sub>2</sub> on benzene.

adsorption on graphene. Specifically, Lazar et al.<sup>14</sup> computed adsorption enthalpies of small organic molecules on coronene and infinite graphene with a range of empirical, density functional theory, and wave function theory methods. For the coronene model, the best agreement with the reference CCSD(T) interaction energies was achieved with a nonlocal optB88-vdW functional (mean error of 0.6 kcal mol<sup>-1</sup>) and SCS(MI)-MP2 method (mean error of 0.4 kcal mol<sup>-1</sup>), although all tested methods were able to reproduce the qualitative ordering of experimentally measured adsorption enthalpies. The latter were best reproduced with a periodic graphene model and *ab initio* molecular dynamics at the optB88-vdW level. Halder et al.<sup>17</sup> demonstrated convergence of interaction energies for two organic electron acceptor molecules adsorbed on graphene with the size of coronene-based models, justifying the use of cluster models. Considering the levels of theory, the SCS-MP2/CBS, BLYP-D3, and AMBER force field all afforded modest accuracy (within several kcal mol<sup>-1</sup>) with respect to the reference MP2.5/CBS/6-31G\*(0.25) values. Very recently, Stachová et al.<sup>18</sup> assessed the performance of several DFT methods for predicting adsorption energies of monolayers of noble gases (Ar, Kr, Xe) and small molecules (N<sub>2</sub>, O<sub>2</sub>, CO, CH<sub>4</sub>, C<sub>2</sub>H<sub>6</sub>, and C<sub>3</sub>H<sub>8</sub>) on free-standing graphene and graphene on a Pt(111) support. Both high-level RPA and fixed-node diffusion Monte Carlo computations and previously published experimental results were used as benchmarks. For bare (unsupported) graphene, the authors recommended PBE-D3 for adsorption energies and optB86b for geometries. For graphene on Pt(111), the choice of the best approach was found to depend on the strength of the interactions: PBE-D3 for weakly interacting systems (interaction energies below 20 kJ mol<sup>-1</sup>) and optB86b-vdW for physisorptions stronger than 20 kJ mol<sup>-1</sup>.

In this study, we aim to establish the most balanced approach to simulating the adsorption of CO<sub>2</sub> on graphene, pertinent to the development of efficient technologies for carbon dioxide capture and conversion.<sup>19</sup> To address this question, we assessed the performance of diverse electronic structure theory methods across the surface model sizes for the adsorption geometries and energies of CO<sub>2</sub> on graphene. *In silico* findings were corroborated via comparison with the results from two recent experimental studies. In a study by Takeuchi et al.,<sup>20</sup> adsorption of carbon dioxide on a monolayer of epitaxial graphene on a SiC(0001) surface was analyzed by temperature-programmed desorption (TPD) and X-ray photoelectron spectroscopy (XPS). At low CO<sub>2</sub> coverage, the adsorption energy was

found to be 30.1 ± 1.5 kJ mol<sup>-1</sup>, decreasing to 25.4 ± 1.5 kJ mol<sup>-1</sup> at higher coverages. The XPS results indicated blue shifts of the O 1s and C 1s electron binding energies with increasing adsorbate coverage. Additional periodic density functional theory computations using nonlocal van der Waals exchange-correlation functionals suggested that CO<sub>2</sub> is adsorbed parallel to the surface. In a more recent study by Smith and Kay,<sup>21</sup> a binding energy of 26.1 ± 2 kJ mol<sup>-1</sup> was reported for low CO<sub>2</sub> coverage on graphene on a Pt(111) surface. While this value is close to that reported by the first study,<sup>20</sup> the results of reflection adsorption infrared spectroscopy (RAIRS) suggested that CO<sub>2</sub> is instead tilted away from the surface. Furthermore, the vibrational band of the antisymmetric stretch mode of CO<sub>2</sub>, which is located at 2350 cm<sup>-1</sup> at low coverage, is blue-shifted to 2378 cm<sup>-1</sup> upon the transition to higher coverages.

In this study, we test the ability of various simulation approaches to reproduce the reported experimentally measured adsorption energies and analyze the adsorption geometries of carbon dioxide on graphene in a low-coverage regime. Examined methodological approaches span from the smallest possible graphene model, benzene, treated at various approximations to the DFT exchange-correlation functional and at highly accurate wave-function-based methods, to the realistic periodic representation of monolayer graphene alone and on experimentally relevant supports, SiC(0001) and Pt(111), in conjunction with several density functionals.

## COMPUTATIONAL DETAILS

**Chemical Model.** Finite models of graphene investigated here (Figure 1A) can be categorized based on their edge structures and shapes as circular (benzene, coronene, and circumcoronene), zigzag (rhomboid shapes), and armchair (rectangular shapes). For each of these models, three principal adsorption sites (top, hollow, and bridge, shown in Figure 1B for benzene) are considered in parallel (shown in Figure 1B) and orthogonal orientations. In the larger systems, CO<sub>2</sub> is located either near the central C–C bond (for 2 × 2-zigzag, 4 × 4-zigzag, 3 × 2-armchair) or near the central 6-membered ring. Constrained optimizations, in which restrictions to angles were introduced through auxiliary dummy atoms, were performed to preserve the initial adsorption geometries, since they do not necessarily correspond to the local minima on the potential energy surface (PES); the corresponding structures and their energies were then compared to those in the fully relaxed minima, obtained in unconstrained optimizations and confirmed by normal-mode analyses.

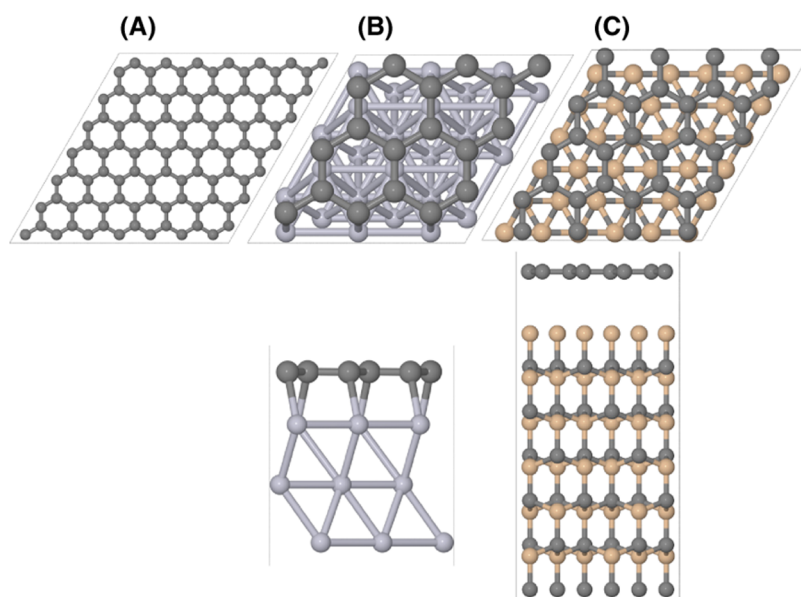


**Figure 2.** Periodic models used in this work. (A) Top view of the  $7 \times 7$  bare graphene model. (B) Top and side views of a graphene  $3 \times 3$  cell placed on top of a three-layer (111)  $3 \times 3$  Pt surface slab. (C) Top and side views of the  $(\sqrt{3} \times \sqrt{3})$ -R30-SiC(0001) unit cell.

**Finite Model.** The following DFT methods in combination with appropriate dispersion corrections were used in geometry and energy computations: generalized gradient approximation functional PBE-D3,<sup>22,23</sup> hybrid-GGA functional B3LYP-D3,<sup>24,25</sup> long-range separated functional  $\omega$ B97X-D3<sup>26</sup> and its nonlocal version  $\omega$ B97X-V<sup>27</sup> for single-point energies, and the double-hybrid functional DSD-BLYP-D3.<sup>28</sup> The latter two functionals were found to be among the best for describing inter- and intramolecular noncovalent interactions.<sup>29</sup> All DFT computations were performed with a recent version of the ORCA program<sup>30</sup> using *very tight* convergence thresholds and the largest DFT grids (keyword: GRID7). A sample input is provided in the [Supporting Information](#). Coupled cluster with singles, doubles, and perturbative triples (CCSD(T)) computations were performed using the XNCC module of the CFOUR program.<sup>31,32</sup> ORCA's capability to function as an external optimizer was utilized to perform geometry optimizations with Cartesian coordinates with and without constraints using the exact same convergence criteria as for the DFT computations. An in-house interface using Atomic Simulation Environment (ASE)<sup>33</sup> was used to transform the gradients between the input orientation and CFOUR's standard orientation. Using ORCA, we have also performed domain local-pair natural orbital coupled cluster with perturbative triples, DLPNO-CCSD(T), computations to obtain interaction energies in conjunction with two default sets of thresholds, *NormalPNO* and *TightPNO*.<sup>34,35</sup> The symmetry-adapted perturbation theory (SAPT)<sup>36–38</sup> computations at a SAPT0 level in conjunction with DFT geometries were performed in the dimer basis for the fragments' wave functions with the resolution-of-the-identity (RI) approximation using Psi4.<sup>39,40</sup> The SAPT0 results are relatively independent of the DFT functional used to obtain the geometries (see [Table S7](#)), thus data based on the PBE-D3 geometries are reported herein.

The interaction energy is computed as the difference between the energies of the optimized dimer and the two monomers in their dimer geometries

$$E_{\text{int}} = E_{\text{graphene}/\text{CO}_2}^D(D) - E_{\text{CO}_2}^D(D) - E_{\text{graphene}}^D(D) \quad (1)$$

where  $E_X^D(D)$  is the energy of the fragment X in the dimer geometry using the dimer basis set. Computations for the monomer fragments are performed using the basis set of the dimer to correct for the basis set superposition error (BSSE). Importantly, computed interaction energies are always slightly lower than the adsorption energies, since the latter contain additional, albeit relatively small in noncovalently bound complexes, relaxation effects (or deformation energy) of the monomers.

**Periodic Model.** Computations on an infinite (periodic) model of graphene were performed using Quantum Espresso<sup>41</sup> with pseudopotentials from the PSLibrary.<sup>42</sup> An energy cutoff of 90 Ry for the plane-wave expansion of the wave function was selected after careful evaluation of the interaction energy dependence on the cutoff value (see [Figure S1](#)). In all systems, a  $3 \times 3 \times 1$   $k$ -point grid was used (see [Table S1](#)). In contrast to the finite cluster systems, no constraints were needed, since initial adsorption geometries were preserved throughout optimizations. The systems were optimized using the default optimization parameters of Quantum Espresso. Computations were performed with the GGA functionals and empirical dispersion corrections, namely, PBE-D3 and B86BPBE-XDM,<sup>43</sup> and with nonlocal van der Waals functionals vdW-DF1,<sup>44</sup> vdW-DF2,<sup>45</sup> optB88-vdW,<sup>46</sup> and optB86b-vdW.<sup>47</sup> For all computations, PBE-derived pseudopotentials were used. Nudged elastic band (NEB)<sup>48–51</sup> computations as implemented in the ASE<sup>33</sup> were performed to find the minimum energy paths between different adsorption sites.

For a bare monolayer of pristine graphene, a  $7 \times 7$  supercell approach with 98 carbon atoms was used ([Figure 2A](#)). For graphene on a platinum support, a  $3 \times 3$  graphene supercell was placed on a  $3 \times 3 \times 3$  Pt(111) supercell ([Figure 2B](#)). The resulting lattice strain for graphene, estimated using the STRAIN structural utility of the Bilbao Crystallographic Server,<sup>52–54</sup> is 0.06354; strain energy, computed at the optB86b level of theory as the difference between the energy of graphene with lattice deformation and the energy at the experimental lattice constant, is 0.77 eV/atom. Although this strain energy per atom is rather high and other adlayer



Table 1. Computed Interaction Energies (in kJ mol<sup>-1</sup>) for CO<sub>2</sub> on Benzene at Various Adsorption Sites and Orientations<sup>c</sup>

Method	Global minima			Local minima (constrained optimisation)			MAD <sup>a</sup>			
				Parallel orientation		Orthogonal orientation		Par.	Ort.	Tot.
				bridge	top	hollow	bridge			
<b>Method//CCSD(T)/def2-TZVP</b>										
DLPNO-CCSD(T)/(TightPNO)/CBS <sup>b</sup>	-10.0	-9.7	-9.3	-9.1	-1.6	-1.7	-2.2	0.0	0.0	0.0
DLPNO-CCSD(T)(TightPNO)/def2-QZVPPD	-9.2	-8.9	-8.6	-8.4	-1.5	-1.4	-1.8	0.8	0.3	0.5
DLPNO-CCSD(T)(NormalPNO)/def2-QZVPPD	-10.2	-9.8	-9.4	-9.4	-1.9	-1.6	-2.4	0.1	0.2	0.2
CCSD(T)-EP2(2/3,MP2) <sup>b</sup>	-10.9	-10.6	-10.2	-10.0	-1.7	-1.7	-2.3	0.9	0.1	0.5
CCSD(T)-EP2(3/4,MP2) <sup>b</sup>	-10.7	-10.4	-10.0	-9.8	-1.7	-1.7	-2.4	0.7	0.1	0.5
CCSD(T)/def2-TZVP	-7.6	-7.2	-6.9	-7.1	-0.4	-0.4	-0.5	2.3	1.4	1.9
DLPNO-CCSD(T)(TightPNO)/def2-TZVP	-7.1	-6.8	-6.5	-6.7	-0.5	-0.5	-0.5	2.8	1.3	2.2
DLPNO-CCSD(T)(NormalPNO)/def2-TZVP	-8.0	-7.8	-7.4	-7.7	-0.8	-0.8	-1.3	1.8	0.9	1.4
SAPT0/jun-cc-pVDZ	-9.0	-8.4	-8.0	-8.2	0.1	0.0	0.2	1.2	2.0	1.5
SAPT0/def2-TZVP	-12.0	-11.5	-11.0	-10.8	-1.0	-1.0	-1.4	1.8	0.7	1.3
SAPT0/def2-QZVPPD	-14.2	-13.7	-13.1	-12.7	-2.1	-2.1	-3.0	3.9	0.6	2.5
SAPT2/def2-QZVPPD	-12.9	-12.5	-12.0	-11.8	-2.9	-2.8	-4.0	2.7	1.4	2.2
SAPT2+/def2-QZVPPD	-12.2	-11.9	-11.4	-11.2	-2.6	-2.6	-3.6	2.1	1.1	1.7
SAPT2+(3)/def2-QZVPPD	-11.7	-11.3	-10.8	-10.8	-2.2	-2.1	-3.0	1.6	0.6	1.2
SAPT2+3/def2-QZVPPD	-12.4	-12.1	-11.6	-11.2	-2.2	-2.1	-2.9	2.3	0.6	1.5
PBE-D3/def2-TZVP	-10.1	-9.7	-9.5	-9.4	-1.7	-1.7	-2.0	0.1	0.1	0.1
B3LYP-D3/def2-TZVP	-10.8	-10.5	-10.1	-9.9	-0.8	-0.8	-1.2	0.8	0.9	0.8
ωB97X-D3/def2-TZVP	-11.3	-10.8	-10.4	-10.2	-0.9	-0.9	-1.4	1.1	0.8	1.0
ωB97X-V/def2-TZVP	-10.7	-10.3	-9.9	-9.9	-1.2	-1.2	-1.8	0.6	0.5	0.5
DSD-BLYP-D3/def2-TZVP	-9.2	-8.8	-8.5	-8.4	-0.7	-0.8	-1.1	0.8	1.0	0.9
<b>Method/def2-TZVP//Method/def2-TZVP</b>										
PBE-D3	-10.2	-9.9	-9.6	-9.5	-1.7	-1.7	-2.1	0.2	0.1	0.2
B3LYP-D3	-10.9	-10.5	-10.2	-10.0	-0.9	-0.9	-1.3	0.9	0.8	0.8
ωB97X-D3	-11.3	-10.9	-10.5	-10.3	-1.0	-1.0	-1.5	1.2	0.7	1.0
ωB97X-V	-10.6	-10.2	-9.8	-9.8	-1.2	-1.2	-1.8	0.6	0.4	0.5
DSD-BLYP-D3	-9.2	-8.8	-8.4	-8.4	-0.8	-0.8	-1.1	0.8	1.0	0.9
<b>Method/def2-QZVPPD//Method/def2-TZVP</b>										
PBE-D3	-10.2	-9.9	-9.7	-9.4	-2.0	-2.0	-2.4	0.3	0.3	0.3
DSD-BLYP-D3	-10.1	-9.8	-9.5	-9.2	-1.4	-1.3	-1.9	0.1	0.3	0.2

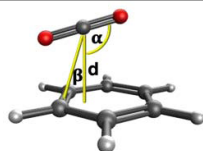
<sup>a</sup>Par. stands for parallel orientation, Ort. stands for orthogonal orientation, and Tot. stands for total for all considered orientations. <sup>b</sup>Here, the aug-cc-pVXZ basis sets were used for extrapolations (see details in the Supporting Information). <sup>c</sup>The cells are colored according to their mean absolute deviation (MAD) with respect to the reference DLPNO-CCSD(T)/(TightPNO)/CBS results. The first column is colored with the averaged total MAD over all geometries (last column).

configurations resulting in lower strain energies are certainly possible, the (3 × 3) domains of graphene on Pt(111) have been observed experimentally<sup>55</sup> and are therefore not only computationally convenient but also realistic models. Adsorption energies do not change significantly when thicker models of the Pt(111) supports are used (see the Supporting Information for details). The two lowest Pt layers were fixed during the optimization. For graphene on a silica carbide support, (√3 × √3)-R30-SiC(0001) model was capped such that Si atoms interact with the graphene layer (Figure 2C). Though this domain was not directly observed in the experiment, it corresponds to the so-called CSG model (covalently bound stretched graphene), which was proposed by Emtsev et al. as a computationally feasible alternative to larger, experimentally detected (6√3 × 6√3) domains.<sup>56</sup> To ensure a low CO<sub>2</sub> adsorption concentration, we created a (2 × 2) supercell from the CSG model. The resulting lattice strain<sup>52–54</sup> for graphene is 0.04410 (the computed strain energy is 0.42 eV/atom). All SiC

layers were frozen during the optimization, except for the top one.

## RESULTS AND DISCUSSION

**Method Assessment: Geometries and Energies for CO<sub>2</sub>⋯Benzene.** We have chosen two experimental studies<sup>20,21</sup> as sources of reference data for our computations. In these works, orientation of the carbon dioxide molecule on graphene is coparallel when graphene is deposited on SiC(0001) and tilted with respect to the graphene surface for Pt(111) support. Correspondingly, we investigated several principal adsorption sites for both orientations (Figure 1B). Initial assessment of diverse density functional and wave function theory methods and basis sets was performed for the smallest possible model system—CO<sub>2</sub>⋯benzene complex—using DLPNO-CCSD(T)-(TightPNO)/CBS level of theory as a reference (Table 1).<sup>34,35</sup> Interaction energies (eq 1) were computed with wave function theory methods in conjunction with the CCSD(T)/def2-TZVP-optimized geometries; density functional theory methods were

**Table 2. Geometrical Parameters across Adsorption Sites of CO<sub>2</sub> on Benzene Computed with Different Electronic Structure Methods<sup>a</sup>**


Method/def2-TZVP	Global minima			Local minima (constrained optimisation)					
	$\alpha, ^\circ$	$\beta, ^\circ$	$d, \text{Å}$	Parallel orientation			Orthogonal orientation		
				bridge	top	hollow	bridge	top	hollow
CCSD(T)	92.5	3.8	3.25	3.24	3.24	3.40	3.41	3.42	3.27
PBE-D3	93.8	1.6	3.30	3.30	3.29	3.47	3.46	3.46	3.36
B3LYP-D3	93.3	2.1	3.25	3.25	3.24	3.40	3.44	3.43	3.29
$\omega$ B97X-D3	93.2	2.2	3.21	3.22	3.21	3.38	3.45	3.46	3.33
DSD-BLYP-D3	92.5	3.2	3.24	3.23	3.23	3.39	3.40	3.40	3.26

<sup>a</sup>The inset figure illustrates these parameters.

**Table 3. Size Dependency of the Interaction Energies (kJ mol<sup>-1</sup>) of CO<sub>2</sub> on Multiple Graphene Models Computed with PBE-D3**

model	no. of carbon atoms	global minima	local minima (constrained optimization)					
			parallel orientation			orthogonal orientation		
			bridge	top	hollow	bridge	top	hollow
benzene	6	-10.2	-9.9	-9.6	-9.5	-1.7	-1.7	-2.1
coronene	24	-13.9	-13.9	-13.2	-12.8	-6.0	-5.8	-6.9
circumcoronene	54	-15.4	-15.4	-14.6	-14.0	-7.6	-7.5	-8.2
2'2-zigzag	16	-13.1	-13.1	-12.3	-11.4	-5.1	-4.9	-4.9
3'3-zigzag	30	-14.3	-14.2	-13.6	-13.1	-6.3	-6.4	n/a <sup>a</sup>
4'4-zigzag	48	-15.2	-15.2	-14.5	-13.8	-7.4	-7.4	-7.8
2'2-armchair	20	-13.3	-13.3	-13.0	-12.2	-5.2	-5.2	-6.2
3'2-armchair	28	-14.4	-14.4	-13.7	-12.8	-6.6	-6.4	-6.9
5'3-armchair	66	-15.5	-15.5	-14.8	-14.0	-7.7	-7.6	-8.3
extrapolated		-16.3	-16.3	-15.6	-14.9	-8.6	-8.6	-9.4

<sup>a</sup>(Constraint) minimum structure that preserved the initial characteristics was not located.

tested in conjunction with the corresponding DFT-optimized geometries. jun-cc-pVDZ basis set, corresponding to the so-called bronze level of SAPT,<sup>36</sup> is used exclusively for SAPT0, while def2-TZVP and def2-QZVPPD basis sets are used with other methods.

Coupled cluster theory results reveal basis set dependence; e.g., the deviations from the reference data become larger (up to 2.8 kJ mol<sup>-1</sup>) when moving from def2-QZVPPD to def2-TZVP. Among the symmetry-adapted perturbation theory approaches, SAPT0/jun-cc-pVDZ results stand out in that positive interaction energies are predicted for orthogonal adsorptions, and the relative stabilities for the parallel adsorptions disagree with the reference DLPNO-CCSD(T)(TightPNO)/CBS//CCSD(T)/def2-TZVP results. All other SAPT-based approaches result in mean absolute deviations between 0.6 and 3.9 kJ mol<sup>-1</sup> relative to the reference, with the disagreement being larger for parallel adsorptions. Finally, all density functionals predict the correct relative energetic order of the adsorption geometries with high accuracy (less than 1.0 kJ mol<sup>-1</sup> deviation from the reference in most cases). Based on mean absolute deviations, performance of the density functionals in this work is generally in line with the findings of an extensive benchmark study by Goerigk et al.,<sup>29</sup> who report the following mean absolute deviations for the S66 test set (in kJ mol<sup>-1</sup>): 1.67 (PBE-D3), 1.09 (B3LYP-D3), 1.00 ( $\omega$ B97X-D3), 0.50 ( $\omega$ B97X-V), and 0.71 (DSD-BLYP-D3). A notable deviation from this trend is the PBE functional, which, according to our results, noticeably outperforms other density functional approximations. Nonetheless, all computed  $E_{\text{int}}$  values are

significantly smaller than the reported experimental adsorption energies for CO<sub>2</sub> on graphene ( $30.1 \pm 1.5$  kJ mol<sup>-1</sup> and  $26.1 \pm 2$  kJ mol<sup>-1</sup>),<sup>20,21</sup> suggesting that larger models might be needed to reproduce these values.

Considering the specific adsorption geometries, parallel orientations are significantly more stable than orthogonal orientations, independent of the computational method. For a given parallel orientation, top and bridge sites are very close in energy, while the hollow site is on average approximately 0.5 kJ mol<sup>-1</sup> less stable. We further analyzed the distance  $d$  between the adsorption site (benzene ring plane) and the CO<sub>2</sub> molecule (carbon or oxygen atom in case of parallel or orthogonal adsorption, respectively); tilt angle  $\alpha$  between the CO<sub>2</sub> axis and the surface plane; and angle  $\beta$  representing an angle between the adsorption site, CO<sub>2</sub> center of mass (i.e., the carbon atom), and its projection onto the surface plane (Table 2). Within the constrained geometries, the bridge and top sites in the parallel orientation feature very similar distances  $d$ , which are consistently larger by approximately 0.17 Å in hollow geometries. The converse is evident for orthogonal orientations, where the hollow adsorption occurs at a shorter distance relative to the top and bridge counterparts. These structural trends reflect the corresponding interaction energies (Table 1): the top and bridge adsorptions are more stable for parallel but less stable for the orthogonal orientations compared to the hollow adsorptions. The global minimum geometries are generally very similar to the bridge parallel adsorption site; however, the CO<sub>2</sub> in the former is slightly shifted toward the center of the ring, as indicated by the  $\beta$  angle.

Compared with the CCSD(T) reference, all density functionals predict qualitatively correct trends. However, PBE-D3 results tend to overestimate  $d$  by 0.05–0.09 Å for all adsorption geometries; this behavior of GGA functionals for covalent bonds has been attributed to their neglect of the Hartree–Fock-like exact exchange,<sup>57</sup> but the reasons can certainly be more complex in the noncovalent case and may include additional many-body effects. Geometries obtained with the global hybrid B3LYP-D3 and the long-range separated  $\omega$ B97X-D3 are closer to the CCSD(T) geometries than those computed using PBE-D3. Finally, double-hybrid functional DSD-BLYP-D3 reproduces the CCSD(T) geometries most accurately, with a maximum deviation of only 0.02 Å.

Overall, the double-hybrid functional DSD-BLYP-D3 predicts geometries and energies that are the closest to the CCSD(T) reference, in line with the recent benchmark study.<sup>29</sup> However, the scaling of its computational cost is less favorable compared to B3LYP-D3 and  $\omega$ B97X-D3, and especially to PBE-D3,<sup>57,58</sup> which predicts excellent energies and good geometries. This factor, while insignificant for a relatively compact benzene...CO<sub>2</sub> complex, can become crucial when moving toward larger and more realistic surface models.

**Size Dependency.** How transferable is the computed interaction energy of carbon dioxide with benzene to the infinite graphene sheet? To address this, we have tested the size dependency of  $E_{\text{int}}$  computed with various DFT methods across a range of cluster models (Figure 1); for clarity, only the PBE-D3 results are detailed further (Table 3; corresponding geometrical parameters and the results of other methods can be found in Tables S4, S5, and S7).

These results suggest that

- (1) Larger surface models lead to more stable clusters independent of the computational method and the adsorption geometry. On average, the interaction energies are lower by 6–8 kJ mol<sup>-1</sup> for the largest considered graphene models compared to the smallest ones. Furthermore, this increase in the stability of CO<sub>2</sub>...graphene complexes is accompanied by shorter interaction distances (see Table S4), albeit to an extent dependent on the adsorption site. A similar correlation between larger graphene models and shorter adsorption distances was reported by Irle et al.<sup>59</sup>
- (2) The relative order of interaction energies does not depend on the system size. For example, the bridge parallel adsorption is always the most stable (optimized under constraint), followed by the top and hollow parallel orientations. Similarly, the hollow adsorption site is the most stable among orthogonal orientations (except for the 2 × 2-zigzag model).
- (3) All larger models (circumcoronene, 3 × 3-zigzag, and 5 × 3-armchair) converge to similar adsorption geometries. For example, all large models feature similar CO<sub>2</sub>...surface distances for the bridge parallel adsorption (see Table S4).
- (4) Geometries of all global minima are similar to each other and very similar to the bridge parallel adsorption.
- (5) The interaction energy is approximately linearly proportional to the inverse size of the surface model (beyond benzene), i.e., the inverse of the number of carbon atoms it contains (PBE-D3 data are shown in Figure 3, while the plots for other methods are given in Figure S2). The linear fit of this data intercepts the  $y$ -axis at  $\lim_{x \rightarrow \infty} m/x + n$ , where

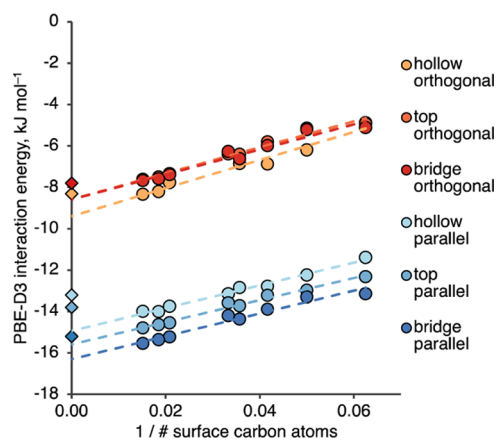


**Figure 3.** PBE-D3 interaction energies of CO<sub>2</sub> plotted vs the inverse of the number of carbon atoms in the underlying finite surface model (circles), linear regression fits of the finite model data points (dashed lines), and corresponding PBE-D3  $E_{\text{int}}$  for the periodic model (diamonds).

$x$  is the number of carbon atoms in the surface model. Similar extrapolation schemes have been established for  $E_{\text{int}}$  of graphene with water (exponential fit),<sup>60</sup> acetone (three-parameter exponential fit),<sup>59</sup> a second graphene layer,<sup>61</sup> and nucleobases<sup>62</sup> (nonlinear two parameter fits). An extensive study of water physisorption on graphene by Brandenburg et al. using such sophisticated many-body electronic structure methods as CCSD(T), random phase approximation, and diffusion Monte Carlo in a periodic setup, questioned the reliability of extrapolated interaction energies.<sup>63</sup> However, Jordan and Heßelmann demonstrated that upon rigorous inclusion of long-range electrostatic effects an excellent agreement is achieved between the aforementioned high-level periodic computations and those obtained using extrapolation from cluster models.<sup>64</sup> Importantly, such an extrapolation scheme gives interaction energies for an artificial, infinitely large graphene model at any quantum chemical method applicable to finite systems (Table 4).

Extrapolated values for the interaction of carbon dioxide with an artificial infinite graphene sheet follow the same trends in terms of preferred adsorption geometries at all levels of theory considered (Table 4). The bridge parallel adsorption site is the most stable and converges with the values obtained for the global minimum adsorptions. The highest  $E_{\text{int}}$  values are obtained with PBE-D3 computations and the lowest with B3LYP-D3. The interaction energies obtained with SAPT0 are sensitive to the basis set but largely independent of the underlying geometries (see also Table S8) and are even lower than the B3LYP-D3 values (Table 4).

**Periodic Models.** In the experimental studies,<sup>20,21</sup> graphene was deposited on substrates, which likely affect its adsorption properties. To elucidate the influence of these supports and verify the reliability of the extrapolation scheme based on finite (cluster) models, we further computed adsorption energies of CO<sub>2</sub> on bare graphene and with SiC(0001) and Pt(111) supports (Table 5).

First, we note that adsorption geometries in the optimized periodic models are relatively similar across the methods and supports and are also close to those obtained with the larger cluster models (see Table S6). For the CO<sub>2</sub> adsorption on unsupported (bare) graphene, dispersion-corrected GGA func-

**Table 4. Extrapolated Interaction Energies ( $\text{kJ mol}^{-1}$ ) of  $\text{CO}_2$  Adsorbed on an Artificial Infinite Graphene Model Computed with Several Density Functionals and SAPTO**

method	global minima	local minima (constrained optimization)					
		parallel orientation			orthogonal orientation		
		bridge	top	hollow	bridge	top	hollow
Method/def2-TZVP//Method/def2-TZVP							
PBE-D3	-16.3	-16.3	-15.6	-14.9	-8.6	-8.6	-9.4
B3LYP-D3	-19.8	-19.8	-18.8	-18.0	-9.5	-9.5	-10.6
$\omega$ B97X-D3	-17.9	-17.8	-16.6	-15.8	-8.4	-8.4	-9.5
$\omega$ B97X-V	-18.6	-18.6	-17.4	-16.7	-9.7	-9.7	-10.4
DSD-BLYP-D3	-18.9	-18.9	-18.0	-17.3	-10.3	-10.3	-11.6
SAPT0/def2-TZVP//Method/def2-TZVP							
PBE-D3	-24.8	-24.8	-23.2	-22.0	-14.2	-14.1	-15.9
B3LYP-D3	-25.7	-25.6	-23.9	-22.7	-14.7	-14.5	-16.5
$\omega$ B97X-D3	-25.6	-25.5	-23.8	-22.6	-14.3	-14.2	-16.1
DSD-BLYP-D3	-27.0	-26.8	-25.1	-23.8	-15.3	-15.2	-18.2
SAPT0/jun-cc-pVDZ//Method/def2-TZVP							
PBE-D3	-20.7	-20.6	-19.3	-18.4	-12.7	-12.7	-14.0
B3LYP-D3	-20.9	-20.9	-19.5	-18.5	-12.9	-12.9	-14.4
$\omega$ B97X-D3	-20.8	-20.7	-19.3	-18.5	-12.7	-12.7	-14.1
DSD-BLYP-D3	-21.4	-21.2	-20.0	-18.9	-13.2	-13.2	-14.9

**Table 5. Interaction Energies (in  $\text{kJ mol}^{-1}$ ) of  $\text{CO}_2$  Adsorbed on Periodic Bare Graphene and on Periodic Single-Layer Graphene Deposited on Silica Carbide and Platinum Supports<sup>a</sup>**

method	local minima (constrained optimization)					
	parallel orientation			orthogonal orientation		
	bridge	top	hollow	bridge	top	hollow
Bare Graphene						
PBE-D3	-15.2	-13.8	-13.2	-7.8	-7.8	-8.3
B86BPBE-XDM	-13.0	-12.3	-11.1	-6.0	-6.0	-6.6
vdW-DF-1	-21.0	-20.6	-20.0	-12.9	-12.9	-13.4
vdW-DF-2	-17.7	-17.2	-16.3	-10.1	-10.0	-10.5
optB88-vdW	-21.5	-20.9	-19.4	-12.5	-12.4	-13.2
optB86b-vdW	-22.5	-21.7	-20.4	-12.7	-12.6	-13.3
Graphene on Pt(111)						
PBE-D3	-15.3 (-0.1)	-14.8 (-1.0)	-13.7 (-0.6)	-10.5 (-2.6)	-9.4 (-1.6)	-10.1 (-1.8)
B86BPBE-XDM	-10.6 (2.5)	-10.4 (1.9)	-8.6 (2.4)	-6.7 (-0.7)	-5.8 (0.2)	-7.9 (-1.3)
vdW-DF1	n/a <sup>d</sup>	-22.7 (-2.1)	n/a <sup>d</sup>	n/a <sup>d</sup>	-15.1 (-2/3)	-13.3 (0.1)
vdW-DF2	n/a <sup>d</sup>	-18.0 (-0.8)	n/a <sup>d</sup>	n/a <sup>d</sup>	n/a <sup>d</sup>	n/a <sup>d</sup>
optTB88-vdW	-24.4 (-2.9)	-24.2 (-3.3)	-22.2 (-2.9)	-14.6 (-2.1)	-14.7 (-2.3)	-15.8 (-2.6)
optB86b-vdW	-25.5 (-3.0)	-24.9 (-3.2)	-23.3 (-2.9)	-15.2 (-2.4)	-15.3 (-2.7)	-16.3 (-3.1)
exp. (low coverage) <sup>21</sup>				-26.1 ± 2		
Graphene on SiC(0001)						
PBE-D3	-14.2 (1.0)	-14.1 (-0.3)	-13.1 (0.1)	-8.4 (-0.6)	-8.3 (-0.5)	-9.1 (-0.8)
B86BPBE-XDM	-9.4 (3.6)	-12.7 (-0.5)	-4.9 (6.2)	-7.4 (-1.4)	-3.9 (2.0)	-8.6 (-2.1)
vdW-DF1	-22.0 (-1.0)	-21.7 (-1.1)	-20.9 (-0.9)	-14.5 (-1.6)	-14.5 (-1.6)	-15.1 (-1.8)
vdW-DF2	-18.3 (-0.6)	-18.0 (-0.8)	-16.8 (-0.5)	-11.1 (-1.0)	-11.1 (-1.1)	-12.1 (-1.6)
optB88-vdW	-22.4 (-0.9)	-22.3 (-1.5)	-20.8 (-1.5)	-13.9 (-1.3)	-13.5 (-1.1)	-14.8 (-1.6)
optB86b-vdW	-23.3 (-0.8)	-22.8 (-1.1)	-21.5 (-1.1)	-14.2 (-1.4)	-14.0 (-1.4)	-14.7 (-1.4)
exp. (low coverage) <sup>20</sup>	-30.1 ± 1.5					
exp. (high coverage) <sup>20</sup>	-25.4 ± 1.5					
Extrapolated (Bare Graphene)						
PBE-D3 <sup>b</sup>	-16.3	-15.6	-14.9	-8.6	-8.6	-9.4
DSD-BLYP-D3 <sup>b</sup>	-18.9	-18.0	-17.3	-10.8	-10.3	-11.6
SAPT0 <sup>c</sup> /PBE-D3 <sup>b</sup>	-20.6	-19.3	-18.4	-12.7	-12.7	-14.0

<sup>a</sup>Numbers in brackets are differences between  $E_{\text{int}}$  on a support vs bare graphene at a given level of theory. Extrapolated  $E_{\text{int}}$  from Table 4 and experimental (exp.) binding energies are shown for convenience. <sup>b</sup>def2-TZVP basis set. <sup>c</sup>jun-cc-pVDZ basis set. <sup>d</sup>Optimization diverged from intended adsorption site.

tionals, PBE-D3 and B86BPBE-XDM, predict  $E_{\text{int}}$  approximately 4 to 9  $\text{kJ mol}^{-1}$  higher (weaker) than the vdW functionals. At the

PBE-D3 level, the periodic results are only 0.8 and 1.8  $\text{kJ mol}^{-1}$  higher than the extrapolated values, validating the reliability of



the extrapolation scheme. Across adsorption geometries, Pt(111) support generally provides between 0.4 and 2.6  $\text{kJ mol}^{-1}$  stabilization of  $\text{CO}_2$  adsorbate with GGA functionals and between 0.5 and 3.3  $\text{kJ mol}^{-1}$  with nonlocal vdW functionals. These results are in a very good agreement with a recent study investigating adsorption of small molecules other than  $\text{CO}_2$  on free-standing Pt(111)-supported graphene.<sup>18</sup> Stabilization on silica carbide is mostly smaller, e.g., 0.3–2.1  $\text{kJ mol}^{-1}$  at the GGA level and 0.5–1.8  $\text{kJ mol}^{-1}$  at the nonlocal vdW level. However, in several orientations, the introduction of supports leads to the weakening of adsorption at the GGA level, particularly with the B86BPBE-XDM method (by up to 6.2  $\text{kJ mol}^{-1}$ ). Overall, nonlocal vdW functionals predict significantly lower adsorption energies on supports, in some cases by over 10  $\text{kJ mol}^{-1}$ , than the GGA DFT functionals. Comparing the two support materials, the values of  $E_{\text{int}}$  on platinum are approximately 1–2  $\text{kJ mol}^{-1}$  lower (more stabilizing) than on silica carbide. Finally, across all tested methods and materials (bare graphene, graphene on Pt(111), and graphene on SiC(0001)), parallel orientations are preferred over orthogonal ones by ca. 5–10  $\text{kJ mol}^{-1}$ , with the bridge parallel geometry having the lowest interaction energies.

Modeling  $\text{CO}_2$  adsorption on supported graphene approaches a more realistic representation of the experimental setup but does not reproduce the experimental adsorption energies and geometries. Correcting the extrapolated PBE-D3 interaction energies for the effects of supports (values in brackets in Table 5) leads to  $-17 \text{ kJ mol}^{-1}$  for graphene deposited on platinum and  $-15.9 \text{ kJ mol}^{-1}$  for graphene on silica carbide, as opposed to the experimental values<sup>20,21</sup> of  $-26.1 \pm 2$  and  $-30.1 \pm 1.5 \text{ kJ mol}^{-1}$ , respectively. In fact, while other methods, such as nonlocal van der Waals periodic computations ( $-25.1 \text{ kJ mol}^{-1}$  on Pt(111) and  $-23.3 \text{ kJ mol}^{-1}$  on SiC(0001) for bridge parallel orientation at the optB86b-vdW level) or extrapolated SAPT0 values corrected for the support effects (e.g.,  $-23.6 \text{ kJ mol}^{-1}$  on Pt(111) and  $-21.6 \text{ kJ mol}^{-1}$  on SiC(0001) for bridge parallel orientation using the optB88-vdW corrections), predict more stable adsorptions, i.e., are closer to the experimental values, none of the methods reproduces the key experimental observations—that  $\text{CO}_2$  adsorbs on Pt-supported graphene in a tilted manner (corresponding to the orthogonal orientation in our models) and that adsorption on graphene on silica carbide in low-coverage regime is more exothermal than on a platinum support. Overall, these findings are in a stark contrast to the results obtained by Stachová et al.,<sup>18</sup> whose DFT results are within only 1.9  $\text{kJ mol}^{-1}$  in terms of mean absolute errors from experiment.

**Potential Energy Surface Scans.** To further explore the intricacies of carbon dioxide orientation once it is adsorbed on graphene, we computed the minimum energy paths that connect the bridge parallel adsorption geometries with all three orthogonal orientations by using the nudged elastic band approach at the optB86b level of theory for  $\text{CO}_2$  on bare graphene (Figure 4). All three minimum energy paths are rather similar and reflect the differences in the interaction energies at the corresponding adsorption sites (Table 5). This overall picture does not change when using the PBE-D3 instead (see Figure S4); interaction energy surface scans for the rotation of  $\text{CO}_2$  adsorbed on benzene for all three adsorption sites, computed using the symmetry-adapted perturbation theory, are also provided in the Supporting Information.

**Vibrational Effects.** Experimental measurements do not give adsorption energetics in terms of interaction energies, but rather 0 K adsorption enthalpies, which contain changes in

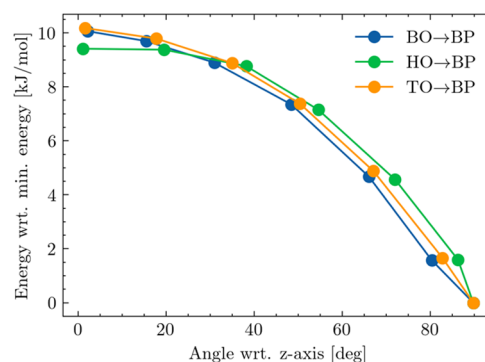


**Figure 4.** Minimum energy paths are computed with the nudged elastic band approach. The paths connect the bridge parallel adsorption site (BP) with the three orthogonally oriented adsorption sites: bridge orthogonal (BO), hollow orthogonal (HO), and top orthogonal (TO).

vibrational zero-point energies.<sup>65</sup> We have accounted for the latter using the harmonic oscillator approximation (see details in the Supporting Information). Since the second-order geometrical derivatives were computed numerically, only the most stable bridge parallel geometry was considered for the optB86b-vdW functional. We arrived at an adsorption enthalpy of  $\Delta H_{\text{ads}} = -21.7 \text{ kJ mol}^{-1}$ , a rather small correction of  $+0.8 \text{ kJ mol}^{-1}$  to an interaction energy of  $-22.5 \text{ kJ mol}^{-1}$  (the deformation energy is negligible). The main reason for the small vibrational effects is due to weak physisorption, which leaves the normal modes almost undisturbed with respect to free  $\text{CO}_2$ .

## CONCLUSIONS

In search of an optimal methodological approach to modeling the adsorption of  $\text{CO}_2$  on graphene, the ability of various density functional theory and wave function theory methods, as well as finite and periodic models, to reproduce experimental adsorption energies of carbon dioxide on graphene has been probed. For the smallest model, benzene, a comparison with the gold standard of quantum chemistry, CCSD(T), shows that the double-hybrid DSD-BLYP-D3 functional performs the best, in accordance with previous benchmarks. The dispersion-corrected generalized gradient approximation method, PBE-D3, also yields exceptionally good interaction energies and reasonably good geometries, while also being 35 times faster than the double-hybrid computation.<sup>58</sup> For a series of cluster models of pristine graphene (up to 66 carbon atoms), a linear fit extrapolating computed interaction energies of  $\text{CO}_2$  to infinity allows the results of periodic computations to be closely reproduced at a given level of theory. This scheme represents a simple yet powerful tool for obtaining accurate interaction energies for  $\text{CO}_2$  with infinite graphene from a few relatively inexpensive cluster computations. Surprisingly, interaction energies, computed for  $\text{CO}_2$  adsorbed on periodic bare graphene, differ by up to 10  $\text{kJ mol}^{-1}$  between dispersion-corrected GGA functionals and nonlocal van der Waals functionals. The lowest and closest to the experiment interaction energies are obtained with the latter in a periodic setting and with the symmetry-adapted perturbation theory using the extrapolation scheme from the cluster models. Correcting these results for the presence of SiC(0001) and Pt(111) supports, as well as for vibrational effects, leads to a rather minor change of 1–2  $\text{kJ mol}^{-1}$ . Most notably, across all tested theoretical procedures, graphene models, and supports, the parallel adsorption mode of carbon dioxide is energetically



preferred over the orthogonal (tilted) one. Thus, the experimental observation that CO<sub>2</sub> adsorbs on Pt-supported graphene in a tilted manner remains unreproduced *in silico*. Re-examination of this experimental result and further expansion of the computational models to include the influence of pressure and concentration, account for dynamic effects, possible island formation (even at low temperatures and concentrations), and structural defects in bare graphene and kinks in the supports might resolve this disagreement in the future.

In this study, we have demonstrated that even for such a seemingly simple system as CO<sub>2</sub> physisorbed on a polyaromatic hydrocarbon interaction energies vary significantly depending on the chosen electronic structure theory, basis set, and computational model of graphene. While “gold standards” of quantum chemistry can be used as benchmarks for small, finite systems, choosing reliable approaches for periodic systems ultimately necessitates more experimental data, measured *ceteris paribus*.

## ■ ASSOCIATED CONTENT

### Data Availability Statement

Geometries of the periodic systems are freely available from <https://github.com/hits-ccc/CO2-on-Graphene-Structures>.

### SI Supporting Information

The Supporting Information is available free of charge at <https://pubs.acs.org/doi/10.1021/acsomega.3c03251>.

Data on sample input of constrained optimization, plane-wave and k-point dependence of the interaction energies, lattice parameters of the periodic systems, influence of the number of Pt(111) layers, basis set extrapolation, additional methods, size-dependent geometrical parameters, size-dependent interaction energies, extrapolations of interaction energies toward infinite graphene sheet, coupled cluster and higher-order SAPT interaction energies with larger basis sets, vibrational corrections and adsorption enthalpies, minimum energy paths, and SAPT0 energy decomposition analysis. (PDF)

Electronic energies of the studied complexes and raw data, used to create the tables (XLSX)

Geometries of the studied complexes (finite models) (XYZ)

## ■ AUTHOR INFORMATION

### Corresponding Authors

Christopher Ehlert – Heidelberg Institute for Theoretical Studies (HITS gGmbH), 69118 Heidelberg, Germany; Interdisciplinary Center for Scientific Computing (IWR), Heidelberg University, 69120 Heidelberg, Germany; Email: [christopher.ehlert@h-its.org](mailto:christopher.ehlert@h-its.org)

Ganna Gryn'ova – Heidelberg Institute for Theoretical Studies (HITS gGmbH), 69118 Heidelberg, Germany; Interdisciplinary Center for Scientific Computing (IWR), Heidelberg University, 69120 Heidelberg, Germany; [orcid.org/0000-0003-4229-939X](https://orcid.org/0000-0003-4229-939X); Email: [ganna.grynova@h-its.org](mailto:ganna.grynova@h-its.org)

### Author

Anna Piras – Heidelberg Institute for Theoretical Studies (HITS gGmbH), 69118 Heidelberg, Germany; Interdisciplinary Center for Scientific Computing (IWR), Heidelberg University, 69120 Heidelberg, Germany; [orcid.org/0000-0002-1528-8874](https://orcid.org/0000-0002-1528-8874)

Complete contact information is available at: <https://pubs.acs.org/10.1021/acsomega.3c03251>

## Author Contributions

C.E.: investigation, methodology, formal analysis, visualization, writing – initial draft, review, and editing; A.P.: investigation, formal analysis, writing – review, and editing; G.G.: conceptualization, supervision, formal analysis, visualization, funding acquisition, writing – review, and editing.

## Notes

The authors declare no competing financial interest.

## ■ ACKNOWLEDGMENTS

The authors gratefully acknowledge the Klaus Tschira Foundation for financial and administrative support, as well as the state of Baden-Württemberg through bwHPC (JUSTUS 2), the Interdisciplinary Center for Scientific Computing (IWR) of Heidelberg University, and the Heidelberg Institute for Theoretical Studies (HITS gGmbH) for computational resources. The authors also thank Dr. John Lindner for proofreading this manuscript and assisting with the TOC image.

## ■ REFERENCES

- (1) Novoselov, K. S.; Geim, A. K.; Morozov, S. V.; Jiang, D.; Zhang, Y.; Dubonos, S. V.; Grigorieva, I. V.; Firsov, A. A. Electric Field Effect in Atomically Thin Carbon Films. *Science* **2004**, *306*, 666–669.
- (2) Georgakilas, V.; Otyepka, M.; Bourlino, A. B.; Chandra, V.; Kim, N.; Kemp, K. C.; Hobza, P.; Zboril, R.; Kim, K. S. Functionalization of Graphene: Covalent and Non-Covalent Approaches, Derivatives and Applications. *Chem. Rev.* **2012**, *112*, 6156–6214.
- (3) Yu, X.; Cheng, H.; Zhang, M.; Zhao, Y.; Qu, L.; Shi, G. Graphene-Based Smart Materials. *Nat. Rev. Mater.* **2017**, *2*, 17046.
- (4) Shao, Y.; Wang, J.; Wu, H.; Liu, J.; Aksay, I. A.; Lin, Y. Graphene Based Electrochemical Sensors and Biosensors: A Review. *Electroanalysis* **2010**, *22*, 1027–1036.
- (5) Schedin, F.; Geim, A. K.; Morozov, S. V.; Hill, E. W.; Blake, P.; Katsnelson, M. I.; Novoselov, K. S. Detection of Individual Gas Molecules Adsorbed on Graphene. *Nat. Mater.* **2007**, *6*, 652–655.
- (6) Singh, E.; Meyyappan, M.; Nalwa, H. S. Flexible Graphene-Based Wearable Gas and Chemical Sensors. *ACS Appl. Mater. Interfaces* **2017**, *9*, 34544–34586.
- (7) Choi, J. H.; Lee, J.; Byeon, M.; Hong, T. E.; Park, H.; Lee, C. Y. Graphene-Based Gas Sensors with High Sensitivity and Minimal Sensor-to-Sensor Variation. *ACS Appl. Nano Mater.* **2020**, *3*, 2257–2265.
- (8) Yuan, W.; Shi, G. Graphene-Based Gas Sensors. *J. Mater. Chem. A* **2013**, *1*, 10078–10091.
- (9) Piras, A.; Ehlert, C.; Gryn'ova, G. Sensing and Sensitivity: Computational Chemistry of Graphene-Based Sensors. *WIREs Comput. Mol. Sci.* **2021**, *11*, No. e1526.
- (10) Leenaerts, O.; Partoens, B.; Peeters, F. M. Adsorption of H<sub>2</sub>O, NH<sub>3</sub>, CO, NO<sub>2</sub>, and NO on Graphene: A First-Principles Study. *Phys. Rev. B* **2008**, *77*, No. 125416.
- (11) Huang, B.; Li, Z.; Liu, Z.; Zhou, G.; Hao, S.; Wu, J.; Gu, B.-L.; Duan, W. Adsorption of Gas Molecules on Graphene Nanoribbons and Its Implication for Nanoscale Molecule Sensor. *J. Phys. Chem. C* **2008**, *112*, 13442–13446.
- (12) Takeuchi, K.; Yamamoto, S.; Hamamoto, Y.; Shiozawa, Y.; Tashima, K.; Fukidome, H.; Koitaya, T.; Mukai, K.; Yoshimoto, S.; Suemitsu, M.; Morikawa, Y.; Yoshinobu, J.; Matsuda, I. Adsorption of CO<sub>2</sub> on Graphene: A Combined TPD, XPS, and vdW-DF Study. *J. Phys. Chem. C* **2017**, *121*, 2807–2814.
- (13) Tit, N.; Said, K.; Mahmoud, N. M.; Kouser, S.; Yamani, Z. H. Ab-Initio Investigation of Adsorption of CO and CO<sub>2</sub> Molecules on Graphene: Role of Intrinsic Defects on Gas Sensing. *Appl. Surf. Sci.* **2017**, *394*, 219–230.

- (14) Lazar, P.; Karlický, F.; Jurečka, P.; Kocman, M.; Otyepková, E.; Šafářová, K.; Otyepka, M. Adsorption of Small Organic Molecules on Graphene. *J. Am. Chem. Soc.* **2013**, *135*, 6372–6377.
- (15) Staemmler, V. The Cluster Approach for the Adsorption of Small Molecules on Oxide Surfaces. In *Theoretical Aspects of Transition Metal Catalysis*; Frenking, G., Ed.; Topics in Organometallic Chemistry; Springer: Berlin, 2005; Vol. 12.
- (16) Perdew, J. P.; Schmidt, K. Jacob's Ladder of Density Functional Approximations for the Exchange-Correlation Energy. *AIP Conf. Proc.* **2001**, *577*, 1–20.
- (17) Haldar, S.; Kolář, M.; Sedlák, R.; Hobza, P. Adsorption of Organic Electron Acceptors on Graphene-like Molecules: Quantum Chemical and Molecular Mechanical Study. *J. Phys. Chem. C* **2012**, *116*, 25328–25336.
- (18) Stachová, M.; Dubecký, M.; Karlický, F. Adsorption of Atomic and Molecular Monolayers on Pt-Supported Graphene. *Chem. Phys.* **2023**, *564*, No. 111713.
- (19) Chin, B.; Loy, A. C. M.; Cheah, K. W.; Chan, Y. H.; Lock, S. S. M.; Yiin, C. L. Graphene-Based Nanomaterials for CO<sub>2</sub> Capture and Conversion. In *Nanomaterials for Carbon Dioxide Capture and Conversion Technologies*; Mazari, S. A.; Mubarak, N. M.; Tripathi, M., Eds.; Curtin Research Publications, 2023; pp 211–243.
- (20) Takeuchi, K.; Yamamoto, S.; Hamamoto, Y.; Shiozawa, Y.; Tashima, K.; Fukidome, H.; Koitaya, T.; Mukai, K.; Yoshimoto, S.; Suemitsu, M.; et al. Adsorption of CO<sub>2</sub> on Graphene: a Combined TPD, XPS, and vdW-DF Study. *J. Phys. Chem. C* **2017**, *121*, 2807–2814.
- (21) Smith, R. S.; Kay, B. D. Desorption Kinetics of Carbon Dioxide From a Graphene-Covered Pt(111) Surface. *J. Phys. Chem. A* **2019**, *123*, 3248–3254.
- (22) Perdew, J. P.; Burke, K.; Ernzerhof, M. Generalized Gradient Approximation Made Simple. *Phys. Rev. Lett.* **1996**, *77*, 3865–3868.
- (23) Perdew, J. P.; Burke, K.; Ernzerhof, M. Erratum: Generalized Gradient Approximation Made Simple. *Phys. Rev. Lett.* **1997**, *78*, 1396.
- (24) Becke, A. D. Density-Functional Thermochemistry. III. The Role of Exact Exchange. *J. Chem. Phys.* **1993**, *98*, 5648–5652.
- (25) Stephens, P. J.; Devlin, F. J.; Chabalowski, C. F.; Frisch, M. J. Ab Initio Calculation of Vibrational Absorption and Circular Dichroism Spectra Using Density Functional Force Fields. *J. Phys. Chem. A* **1994**, *98*, 11623–11627.
- (26) Lin, Y.-S.; Li, G.-D.; Mao, S.-P.; Chai, J.-D. Long-Range Corrected Hybrid Density Functionals with Improved Dispersion Corrections. *J. Chem. Theory Comput.* **2013**, *9*, 263–272.
- (27) Mardirossian, N.; Head-Gordon, M. ωB97X-V: A 10-Parameter, Range-Separated Hybrid, Generalized Gradient Approximation Density Functional with Nonlocal Correlation, Designed by a Survival-of-the-Fittest Strategy. *Phys. Chem. Chem. Phys.* **2014**, *16*, 9904–9924.
- (28) Kozuch, S.; Gruzman, D.; Martin, J. M. L. DSD-BLYP: A General Purpose Double Hybrid Density Functional Including Spin Component Scaling and Dispersion Correction. *J. Phys. Chem. C* **2010**, *114*, 20801–20808.
- (29) Goerigk, L.; Hansen, A.; Bauer, C.; Ehrlich, S.; Najibi, A.; Grimme, S. A Look at the Density Functional Theory Zoo with the Advanced GMTKN55 Database for General Main Group Thermochemistry, Kinetics and Noncovalent Interactions. *Phys. Chem. Chem. Phys.* **2017**, *19*, 32184–32215.
- (30) Neese, F. Software Update: the ORCA Program System, Version 4.0. *WIREs Comput. Mol. Sci.* **2018**, *8*, No. e1327.
- (31) Matthews, D. A.; Stanton, J. F. Non-Orthogonal Spin-Adaptation of Coupled Cluster Methods: A New Implementation of Methods Including Quadruple Excitations. *J. Chem. Phys.* **2015**, *142*, No. 064108.
- (32) Matthews, D. A.; Cheng, L.; Harding, M. E.; Lipparini, F.; Stopkowicz, S.; Jagau, T.-C.; Szalay, P. G.; Gauss, J.; Stanton, J. F. Coupled-Cluster Techniques for Computational Chemistry: The CFOUR Program Package. *J. Chem. Phys.* **2020**, *152*, No. 214108.
- (33) Larsen, A. S.; Mortensen, J. J.; Blomqvist, J.; Castelli, I. E.; Christensen, R.; Dulak, M.; Friis, J.; Groves, M. N.; Hammer, B.; Hargus, C.; et al. The Atomic Simulation Environment—a Python Library for Working with Atoms. *J. Phys.: Condens. Matter* **2017**, *29*, No. 273002.
- (34) Riplinger, C.; Neese, F. An Efficient and Near Linear Scaling Pair Natural Orbital Based Local Coupled Cluster Method. *J. Chem. Phys.* **2013**, *138*, No. 034106.
- (35) Riplinger, C.; Sandhoefer, B.; Hansen, A.; Neese, F. Natural Triple Excitations in Local Coupled Cluster Calculations with Pair Natural Orbitals. *J. Chem. Phys.* **2013**, *139*, No. 134101.
- (36) Parker, T. M.; Burns, L. A.; Parrish, R. M.; Ryno, A. G.; Sherrill, C. D. Levels of Symmetry Adapted Perturbation Theory (SAPT). I. Efficiency and Performance for Interaction Energies. *J. Chem. Phys.* **2014**, *140*, No. 094106.
- (37) Szalewicz, K. Symmetry-Adapted Perturbation Theory of Intermolecular Forces. *WIREs Comput. Mol. Sci.* **2012**, *2*, 254–272.
- (38) Hohenstein, E. G.; Sherrill, C. D. Wavefunction Methods for Noncovalent Interactions. *WIREs Comput. Mol. Sci.* **2012**, *2*, 304–326.
- (39) Parrish, R. M.; Burns, L. A.; Smith, D. G. A.; Simmonett, A. C.; DePrince, A. E.; Hohenstein, E. G.; Bozkaya, U.; Sokolov, A. Y.; Remigio, R. D.; Richard, R. M.; et al. Psi4 1.1: An Open-Source Electronic Structure Program Emphasizing Automation, Advanced Libraries, and Interoperability. *J. Chem. Theory Comput.* **2017**, *13*, 3185–3197.
- (40) Smith, D. G. A.; Burns, L. A.; Simmonett, A. C.; Parrish, R. M.; Schieber, M. C.; Galvelis, R.; Kraus, P.; Kruse, H.; Remigio, R. D.; Alenaizan, A.; et al. Psi4 1.4: Open-Source Software for High-Throughput Quantum Chemistry. *J. Chem. Phys.* **2020**, *152*, No. 184108.
- (41) Giannozzi, P.; Baseggio, O.; Bonfà, P.; Brunato, D.; Car, R.; Carnimeo, I.; Cavazzoni, C.; de Gironcoli, S.; Delugas, P.; Ruffino, F. F.; et al. Quantum ESPRESSO toward the Exascale. *J. Chem. Phys.* **2020**, *152*, No. 154105.
- (42) Dal Corso, A. Pseudopotentials Periodic Table: From H to Pu. *Comput. Mater. Sci.* **2014**, *95*, 337–350.
- (43) Otero-de-la-Roza, A.; Johnson, E. R. Non-Covalent Interactions and Thermochemistry Using XDM-Corrected Hybrid and Range-Separated Hybrid Density Functionals. *J. Chem. Phys.* **2013**, *138*, No. 204109.
- (44) Dion, M.; Rydberg, H.; Schröder, E.; Langreth, D. C.; Lundqvist, B. I. Van der Waals Density Functional for General Geometries. *Phys. Rev. Lett.* **2004**, *92*, No. 246401.
- (45) Lee, K.; Murray, E. D.; Kong, L.; Lundqvist, B. I.; Langreth, D. C. Higher-Accuracy Van Der Waals Density Functional. *Phys. Rev. B* **2010**, *82*, No. 081101.
- (46) Klimeš, J.; Bowler, D. R.; Michaelides, A. Chemical Accuracy for the van der Waals Density Functional. *J. Phys.: Condens. Matter* **2010**, *22*, No. 022201.
- (47) Klimeš, J.; Bowler, D. R.; Michaelides, A. Van der Waals Density Functionals Applied to Solids. *Phys. Rev. B* **2011**, *83*, No. 195131.
- (48) Henkelman, G.; Jónsson, H. Improved Tangent Estimate in the Nudged Elastic Band Method for Finding Minimum Energy Paths and Saddle Points. *J. Chem. Phys.* **2000**, *113*, 9978–9985.
- (49) Henkelman, G.; Uberuaga, B. P.; Jónsson, H. A Climbing Image Nudged Elastic Band Method for Finding Saddle Points and Minimum Energy Paths. *J. Chem. Phys.* **2000**, *113*, 9901–9904.
- (50) Kolsbjerg, E. L.; Groves, M. N.; Hammer, B. An Automated Nudged Elastic Band Method. *J. Chem. Phys.* **2016**, *145*, No. 094107.
- (51) Makri, S.; Ortner, C.; Kermode, J. R. A Preconditioning Scheme for Minimum Energy Path Finding Methods. *J. Chem. Phys.* **2019**, *150*, No. 094109.
- (52) Aroyo, M. I.; Perez-Mato, J. M.; Orobengoa, D.; Tasci, E.; de la Flor, G.; Kirov, A. Crystallography online: Bilbao Crystallographic Server. *Bulg. Chem. Commun.* **2011**, *43*, 183–197.
- (53) Aroyo, M. I.; Perez-Mato, J. M.; Capillas, C.; Kroumova, E.; Ivantchev, S.; Madariaga, G.; Kirov, A.; Wondratschek, H. Bilbao Crystallographic Server I: Databases and Crystallographic Computing Programs. *Z. Kristallogr. – Cryst. Mater.* **2006**, *221*, 15–27.
- (54) Aroyo, M. I.; Kirov, A.; Capillas, C.; Perez-Mato, J. M.; Wondratschek, H. Bilbao Crystallographic Server II: Representations of

Crystallographic Point Groups and Space Groups. *Acta Crystallogr., Sect. A* **2006**, *62*, 115–128.

(55) Sutter, P.; Sadowski, J. T.; Sutter, E. Graphene on Pt(111): Growth and Substrate Interaction. *Phys. Rev. B* **2009**, *80*, No. 245411.

(56) Emtsev, K. V.; Speck, F.; Seyller, Th.; Ley, L.; Riley, J. D. Interaction, Growth, and Ordering of Epitaxial Graphene on SiC{0001} Surfaces: A Comparative Photoelectron Spectroscopy Study. *Phys. Rev. B* **2008**, *77*, No. 155303.

(57) Neese, F. Prediction of Molecular Properties and Molecular Spectroscopy with Density Functional Theory: from Fundamental Theory to Exchange-Coupling. *Coord. Chem. Rev.* **2009**, *253*, 526–563.

(58) Neese, F.; Schwabe, T.; Grimme, S. Analytic Derivatives for Perturbatively Corrected “Double Hybrid” Density Functionals: Theory, Implementation, and Applications. *J. Chem. Phys.* **2007**, *126*, No. 124115.

(59) Nishimura, Y.; Tsuneda, T.; Sato, T.; Katouda, M.; Irlle, S. Quantum Chemical Estimation of Acetone Physisorption on Graphene Using Combined Basis Set and Size Extrapolation Schemes. *J. Phys. Chem. C* **2017**, *121*, 8999–9010.

(60) Feller, D.; Jordan, K. D. Estimating the Strength of the Water/Single-Layer Graphite Interaction. *J. Phys. Chem. A* **2000**, *104*, 9971–9975.

(61) Grimme, S.; Mück-Lichtenfeld, C.; Antony, J. Noncovalent Interactions between Graphene Sheets and in Multishell (Hyper)-Fullerenes. *J. Phys. Chem. C* **2007**, *111*, 11199–11207.

(62) Antony, J.; Grimme, S. Structures and Interaction Energies of Stacked Graphene–Nucleobase Complexes. *Phys. Chem. Chem. Phys.* **2008**, *10*, 2722–2729.

(63) Brandenburg, J. G.; Zen, A.; Fitzner, M.; Ramberger, B.; Kresse, G.; Tsatsoulis, T.; Grüneis, A.; Michaelides, A.; Alfê, D. Physisorption of Water on Graphene: Subchemical Accuracy from Many-Body Electronic Structure Methods. *J. Phys. Chem. Lett.* **2019**, *10*, 358–368.

(64) Jordan, K. D.; Heßelmann, A. Comment on “Physisorption of Water on Graphene: Subchemical Accuracy from Many-Body Electronic Structure Methods. *J. Phys. Chem. C* **2019**, *123*, 10163–10165.

(65) Nørskov, J. K.; Studt, F.; Abild-Pedersen, F.; Bligaard, T. The Potential Energy Diagram. In *Fundamental Concepts in Heterogeneous Catalysis*; John Wiley & Sons, 2014; pp 6–25.